Radio Science, Volume 35, Number 5, Pages 1241–1251, September–October 2000

Correcting atmospheric path variations in millimeter wavelength very long baseline interferometry using a scanning water vapor spectrometer

David A. Tahmoush and Alan E. E. Rogers

Haystack Observatory, Massachusetts Institute of Technology, Westford

Abstract. The coherence of very long baseline interferometry (VLBI) at millimeter wavelengths can be improved through the use of a water vapor radiometer (WVR) to estimate the atmospheric path length variations along the line of sight to each antenna. Measurements of the water vapor emission spectrum using a simple scanning WVR have been used to correct the interferometer phases, thereby lowering the rms phase variation and increasing the coherence time. The average improvement in the coherent fringe amplitude of 400 s VLBI scans at 3 mm wavelength was 20% with a general trend of a greater improvement for the scans with larger phase variations. Sampling of the spectrum from 18 to 26 GHz allows separation of the water vapor emission from instrumental effects and from the emission of water droplets in clouds. The observed line profiles favor the Van Vleck-Weisskopf line shape.

1. Introduction

At radio wavelengths the atmospheric refraction is increased and made more variable by the presence of water vapor. Water vapor radiometers (WVR) have been used to measure the "wet" path. Much of the early work [*Elgered et al*., 1991; *Davis et al*., 1993] was concentrated on the absolute calibration of the atmospheric path to improve the accuracy of geodetic very long baseline interferometry (VLBI) measurements. *Linfield et al*. [1996] used WVRs to correct VLBI measurements by reducing fluctuations within scans and between scans. At millimeter wavelengths, VLBI coherence is severely limited by the variations of the atmospheric electrical path length, which are largely due to the flow of water vapor cells through the column of atmosphere in which the radiation from the radio source propagates to each antenna. The changes in path length typically limit the temporal coherence of VLBI at 3 mm wavelength under average conditions and at sites of moderate altitude to ~10 s [*Rogers et al*., 1984].

The same water vapor that increases the refractivity also attenuates the radiation and generates emission by radiative transfer. The water vapor emission covers a wide spectral range and peaks at the line resonance frequencies at 22 and 183 GHz and numerous other lines at higher frequencies. The opacity of a path through the atmosphere is very large at 183 GHz, except at very high sites which are above most of the water vapor, so that we chose to measure the less opaque 22 GHz line to sense the water vapor. The emission and scattering from clouds affects the radiometric temperature but has a very small effect on the path length. With a few assumptions, which are discussed in section 4, it is possible to estimate the atmospheric path due to the water vapor by measuring the spectrum using a simple frequency-switched scanning radiometer. To separate the water vapor signature from radiometer gain drifts and scattering from the liquid water droplets in clouds, a weighted least squares estimate is made of three parameters: a constant, a frequency-squared term, and the amplitude of the theoretical water spectrum.

Copyright 2000 by the American Geophysical Union.

Paper number 2000RS002334.
0048-6604/00/2000RS002334$11.00

2. Instrument Design and Characteristics

Figure 1 shows a block diagram of the WVR. A low-noise amplifier (LNA) covering the 18–26 GHz band is followed by a mixer and an IF amplifier, which covers the range 50–550 MHz. The IF power is measured by a broadband back diode square law detector whose output is digitized by a voltage to frequency converter and time interval frequency counter. The 1 GHz wide double sideband RF response of the WVR can be tuned within the 18–26 GHz band by the yttrium/iron/garnet (YIG) local

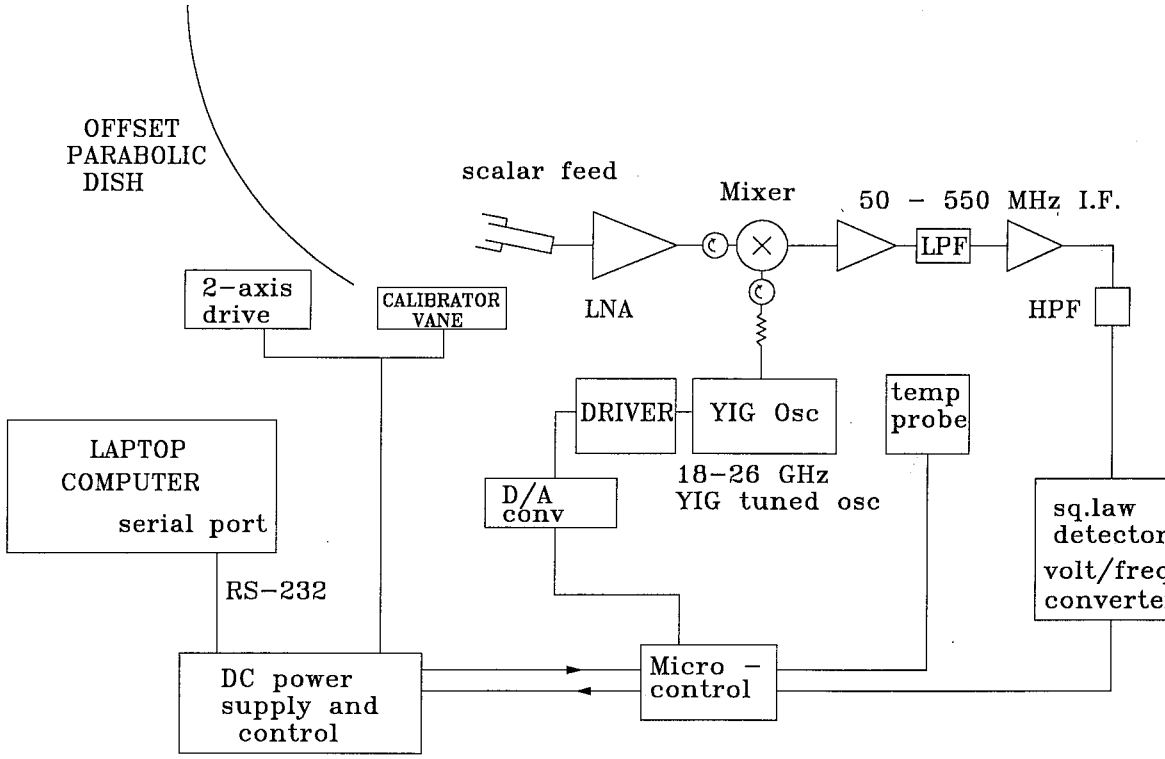

Figure 1. Block diagram of the WVR. LPF and HPF, low- and high-pass filters, respectively.

oscillator. The magnetic field, which determines the YIG frequency, is set using a precision D/A converter and voltage to current conversion operational amplifier. Isolators are employed in the output of the LNA and the local oscillator to minimize the frequency response ripple produced by reflections. Great care is taken to make the circuits as insensitive to temperature as possible by employing low-temperature-coefficient components while maintaining the low cost and simplicity of design. The WVR is controlled by RS232 serial communication. Table 1 lists the instrument characteristics. To minimize input losses, the LNA is connected directly to a probe in the circular waveguide of a scalar feed. The WVR was designed to be flexible in the choice of frequencies to be measured because the optimum choice depends upon the weather, the site, the opacity, and the system characteristics. Variations in the system temperature, gain, and stability with frequency are some of the system characteristics that affect frequency choice.

Table 1. Characteristics of WVR

	Value
Frequency range	18.0–26.5 GHz
System temperature including spillover	350 (upgrading to 190) K
Spillover	~20 K
Antenna beam width 24″ dish	1.5 deg
Total power stability with temperature	1 K K^{-1}
Differential total power stability	~0.1 K GHz^{-1} K^{-1}
YIG warm-up time	30 min
Band-pass variations with frequency	~2 dB peak to peak
IF band pass	50–550 MHz
rms noise in 0.1 s for an individual frequency	0.05 K
rms path length in 30 s between two WVRs	0.1 mm
Weight (excluding dish)	4.3 kg

3. Calibration

Calibration is accomplished using an ambient load and a tipping curve. The ambient load is moved in front of the feed by a computer-controlled arm. The minimum "vane" calibration is performed by measuring the power while looking at the load p_L, at the zenith p_z, and at a low elevation p_θ:

$$p_L = g(t_a + t_r), \tag{1}$$

$$p_z = g(t_z + ce^{-\tau} + t_r + S_z), \tag{2}$$

$$p_\theta = g(t_z r + ce^{-\tau/\sin\theta} + t_r + S_\theta), \tag{3}$$

where

t_a ambient load, ≈300 K;
t_r receiver temperature, ≈350 K;
c cosmic background (CB), ≈3 K;
t_z zenith sky temperature excluding CB ≈ 30 K at 22 GHz;
S_z zenith spillover, ≈25 K;
S_θ low-elevation spillover, ≈15 K;
τ atmospheric opacity;
r ratio of sky temperature at elevation θ to that at the zenith.

These three power measurements at each frequency can be used to solve for the receiver temperature t_r, the sky temperature at the zenith t_z, and the radiometer gain g. We assume fixed values for the antenna spillover at the zenith and at low elevations estimated from the antenna patterns measured in an anechoic chamber. The zenith sky temperature for an isothermal atmosphere at temperature T is equal to $T(1 - e^{-\tau})$. We assume that for an approximately isothermal atmosphere, in which we neglect the Earth's curvature, the opacity varies with secant θ and ratio r can be approximated by

$$r = (1 - e^{-\tau/\sin\theta})/(1 - e^{-\tau}). \tag{4}$$

The equations are nonlinear in τ and are solved using an iterative method which converges rapidly when $1 - e^{-\tau}$ is initially assumed to be equal to τ. Alternately, the gain and receiver temperature can be found from a tipping curve using the method of least squares following a gridded search and linearization of the equations. Following calibration, the sky temperature is measured using the calibrated gain and receiver temperature.

4. Conversion of Water Vapor Spectrum to Path Length

The attenuation spectrum k_ν of the 22 GHz water vapor with the Van Vleck-Weisskopf line shape is given by *Cruz et al.* [1998] as

$$k_\nu = 4.5671 \times 10^{-4}\left(\frac{300}{T}\right)^{3.5} \cdot \exp\left[2.143(1 - 300/T)\right]p_\nu \nu^2 \times \left(\frac{\Delta\nu}{\nu_0}\right)\left[\frac{1}{(\nu - \nu_0)^2 + \Delta\nu^2} + \frac{1}{(\nu + \nu_0)^2 + \Delta\nu^2}\right] \text{km}^{-1}$$

$$\Delta\nu = 2.784 \times 10^{-3}\left[p\left(\frac{300}{T}\right)^{0.6} + 4.8p_\nu\left(\frac{300}{T}\right)^{1.1}\right] \text{GHz}, \tag{5}$$

where

ν frequency, GHz;
ν_0 22.23510 GHz;
p_ν partial pressure of water vapor, mbar;
p pressure of dry air, mbar;
T temperature, K.

Hill [1986] found that the Van Vleck-Weisskopf (VV-W) line shape fit laboratory measurements better than the Gross line shape of the attenuation spectrum used by *Waters* [1976]. Initially, we used the attenuation from Waters but found that the value of pressure required to fit our data was typically 100 mbar lower than expected for the scale height of the water. We consider this to be evidence in favor of the VV-W line shape over the Gross line shape. Therefore we used the VV-W line shape and ignored the effect of other lines and the water vapor continuum [*Rosenkranz*, 1998] because these terms closely approximate a frequency-squared dependence, which cannot be distinguished from the liquid water spectrum.

The relationship between the observed atmospheric brightness temperature due to the atmospheric water vapor and the excess path length can be derived as follows:

The opacity is given by the integral along the path l through the atmosphere by

$$\tau = \int k_\nu \, dl \tag{6}$$

while the excess path length d due to the refractivity N (in units of parts per million) of water vapor is given by

$$d = 10^{-6} \int N\, dl. \tag{7}$$

The water vapor refractivity is related to the partial pressure p_ν and temperature T by

$$N = 3.776 \times 10^5 p_\nu / T^2 \tag{8}$$

from laboratory measurements of refractivity by *Thayer* [1974].

For a thin layer of water vapor at constant temperature T and pressure p the relation between the path d and the brightness of the water line T_B is, from (6), (7), and (8),

$$d = \frac{10^{-6} N T_B}{k_\nu T}, \tag{9}$$

$$d = \frac{3.776 \times 10^5 p_\nu T_B}{k_\nu T^3} \text{ mm}. \tag{10}$$

For example, for $T = 273$ K and $p = 900$ mbar the scale factor is ~4.5 mm per Kelvin at the line center.

The water vapor is measured using a three-parameter least squares fit of the measured sky temperature T_{sky} to a model function

$$T_{\text{sky}}(\nu) = a + b\nu^2 + ch_\nu, \tag{11}$$

where the constant a accounts for small changes in radiometer gain (assuming an approximately constant system temperature), b models the variations in absorption and scattering from water droplets in clouds, mist, and haze, and c models the water vapor line. The constants b and c could be corrected using the gain changes shown in the constant a, but, to first order, that is not necessary if calibrations are done often enough. Here, h_ν is the theoretical spectrum from (5) normalized to unity at the 22.2 GHz line center. As a first approximation, we used fixed values of temperature and pressure obtained from separate observations of the water line, usually made at low elevations, for which the pressure in the model is adjusted to fit the opacity profile. In most cases we found $T = 273$ K and $p = 900$ mbar to be a good fit. If the goal is to measure the path length variations without the need for absolute path, the pressure for which h_ν is calculated should correspond to the altitude where most of the water vapor irregularities occur. In this case the value of pressure is found for which h_ν fits the observed spectral profile of the variations. More complex models using multiple pressure layers, atmospheric profiling, and fitting of the spectra of the irregularities could be used and are currently being tested.

The need to estimate the three parameters a, b, and c increases the statistical noise in the estimate of the water vapor. For 30 uniformly spaced frequencies from 18 to 26 GHz and water vapor at 273 K and 900 mbar the standard deviation of c from the covariance matrix is $0.65^{1/2}$ for unit radiometer noise so that the noise for a 3 s scan is

$$0.65^{1/2}(T_{\text{sky}} + T_r) B^{-1/2} \tau^{-1/2} \approx 0.04 \text{ K} \approx 0.2 \text{ mm} \tag{12}$$

for $T_{\text{sky}} + T_r \approx 350$ K, $B = 500$ MHz. The τ in (12) is the integration time per spectral point and was chosen to be 0.1 s. If both clouds and gain variations could be ignored, we would only need to estimate c and the theoretical noise would be reduced by a factor of 4. The upgrade to the current WVR design using lower noise amplifiers (see Table 1) will improve the sensitivity by a factor of 2 by halving the receiver noise temperature.

5. Error Sources

5.1. Beam Mismatch

The radio waves from a point source propagate through a column of the atmosphere whose diameter D_{col} is equal to that of the receiving dish within the near field (approximately $D_{\text{ant}}^2/(2\lambda)$). Farther away at the beam "waist" the column diameter increases by the diameter of the first Fresnel zone. In the far field of the antenna only the water vapor in the first Fresnel zone has a significant effect on the path delay.

$$\begin{aligned} D_{\text{col}} &\approx D_{\text{ant}} \qquad r < D_{\text{ant}}^2/(2\lambda) \\ &\approx \sqrt{2r\lambda} \qquad r > D_{\text{ant}}^2/(2\lambda). \end{aligned} \tag{13}$$

For a 10 m diameter antenna typical of that used for VLBI at a 3 mm wavelength the transition from near to far field occurs at a distance of 17 km. This is above most of the water vapor, for which the scale height is typically only a few kilometers.

We chose a 60 cm diameter satellite TV offset parabolic dish for our WVR. The beam width of the scalar feed that illuminates the dish decreases with increasing frequency, resulting in an almost constant outgoing beam width of 1.5° from 18 to 26 GHz. The WVR beam can only perfectly match the beam of a 10 m diameter antenna at a distance of 400 m. A better beam match could be obtained by using the

VLBI dish for the WVR. In this case the beams could be made to match out to the far field at 1.3 cm wavelength or out to 4 km. Beyond 4 km the 22 GHz beam diverges from the 100 GHz beam. The effect of beam mismatch is to reduce the correlation of the WVR-estimated path variations with the actual variations in the propagation. The amount of decorrelation can be estimated from the structure function D [*Truehaft and Lanyi*, 1987]

$$D(\tau) = \langle [d(t - \tau) - d(t)]^2 \rangle, \tag{14}$$

where d is the path length, t is time, and τ is time interval. For frozen flow with velocity v the temporal and spatial structure functions are related by substituting the baseline length, $b = \tau v$. For spatial scales of order 100 m or timescale of 10 s for $v = 10$ m s^{-1} and average conditions at sea level, the structure function D in units of m^2 as a function of baseline b in meters is

$$D^{1/2}(b) \approx 7 \times 10^{-6} b^{5/6} \approx 0.3 \text{ mm} \tag{15}$$

for 100 m baseline. The constant is between that obtained by *Armstrong and Sramek* [1982] at the Very Large Array (VLA) in June and that obtained by *Carilli and Holdaway* [1999] in January at the VLA.

The $\frac{5}{6}$ power law is associated with three-dimensional (3-D) turbulence and holds only for spatial scales less than the outer scale of the irregularities, which is ~1 km. Beyond the outer scale the structure function increases more slowly, and the path length variations become uncorrelated, reaching an rms value of ~3 mm at each site. See, for example, the root phase structure function measured at the VLA by *Carilli and Holdaway* [1999]. From our experience and examples in the literature the rms path varies by more than a factor of 4. Conditions are the best on cold winter nights and the worst on humid summer days. Comparing connected element interferometry with VLBI for a wide range of conditions, the path length variations over a 100 m baseline will be approximately 10% of the variation on a long baseline. For water vapor 3 km away, 100 m corresponds to an angle of ~2°, so that an angular error of 2° will reduce the correlation to 90% and result in a rms error of 0.3 mm under average conditions. In a separate experiment performed with two colocated WVRs we found that the correlation of the atmospheric variations on a timescale of 150 s and shorter decreased by ~40% when the beams are separated by 4°. In the same experiments, done during summer at the Haystack Observatory in Massachusetts, it was noted that angular offsets in the direction of the wind resulted in a lead or lag. In that case the peak of the correlation was offset in time with little reduction in amplitude, consistent with the model of frozen turbulent flow. The error due to beam offsets and mismatch has been extensively modeled by *Linfield and Wilcox* [1993], who concluded that a 50 m offset would allow calibration of only 80% of the tropospheric path variations on a timescale of 100 s and would not allow much useful calibration on 10 s timescales. This is consistent with our experience. The loss of correlation with only small angular separations emphasizes the importance of minimizing the beam mismatch. Beams could be most closely matched by locating the WVR at the focus of the VLBI antenna. Unfortunately, there are technical and practical difficulties associated with using the VLBI dish for the WVR. Mounting the largest possible WVR dish on the back of the VLBI subreflector or on the edge of the VLBI dish is a practical compromise. The issue of obtaining better beam match becomes more important at short timescales. The noise in our WVRs limited their usefulness to timescales longer than 10 s.

Table 2. Retrieval Scale Change With Pressure for Uniform and Nonuniform Frequency Coverage From 18 to 26 GHz

Pressure, mbar	Scale Factor at Line Center, mm K^{-1}	Retrieval Scale Error			
		18–26 GHz	18–20 and 24–26 GHz	18, 24, and 26 GHz	18 GHz
400	3.20	1.66	0.93	1.00	1.38
500	3.43	1.54	1.03	1.09	1.28
600	3.67	1.40	1.07	1.11	1.20
700	3.91	1.26	1.07	1.10	1.13
800	4.16	1.12	1.04	1.05	1.06
900	4.41	1.00	1.00	1.00	1.00
1000	4.65	0.89	0.94	0.93	0.95

5.2. Height of Water Vapor Variations

If the water vapor variations occur at a temperature or pressure different from that used to calculate the model function h_ν, there will be a scale factor error in the retrieval of the path delay. Table 2 shows the scale factor for the retrieval of path length based on the line shape h_ν and intensity for a uniform layer of water vapor at various pressures. A temperature of 273 K and partial water vapor pressure of 5 mbar were assumed for the water vapor at 900 mbar. A

lapse rate of -6.5 K km^{-1} combined with a pressure scale height of 8 km were used to derive the model temperatures for other values of pressure. Table 2 also lists the errors in the path length, which will occur when the line shape of the 900 mbar model is used to retrieve the path length for model layers at other pressures. A retrieval scale error greater than 1 in Table 2 means that the WVR will overestimate the path length. For reference, the last column shows the retrieval scale error using a single-frequency system. The major deficiency of a single-frequency WVR is the inability to distinguish between clouds, spillover, other sources of broadband radiometric temperature variations, and the water line.

The scale factor error which results from an error in the assumed temperature is approximately 0.8% per Kelvin and is a much smaller source of error. The line width and hence the scale factor have a weak dependence on the assumed partial pressure of the water. The error in retrieval is only $\sim$0.5% per millibar. It is possible to reduce the sensitivity of the retrieval to a change in the altitude of the water vapor by selecting the frequencies to avoid the region around the line center at 22.235 GHz. This method of reducing the pressure sensitivity by carefully choosing the observed frequencies is well known in water vapor radiometry. For example, *Elgered et al*. [1991] selected frequencies around 20.7 and 31.4 GHz for a two-frequency WVR. Avoiding frequencies within ± 2 GHz of the line center increases the noise in the path length measurement by a factor of 2. A search for a set of frequencies which minimizes simultaneously the path length measurement noise and the variation of retrieval scale with the height of the water vapor found that a good choice is frequencies at 18, 24, and 26 GHz. In this case the noise is only increased by 3%. However, it may be advantageous to cover more than three frequencies, as spreading out the frequencies helps reduce some instrumental effects. The choice of frequencies can be optimized for a given set of observations, but if there are simultaneous water vapor variations at ground level and at high altitudes, the errors resulting from a scale error can only be avoided by a careful selection or weighting of the frequencies. Good performance and lower noise might be obtained on the wings of the 183 GHz water line, avoiding frequencies near the line center, but the high opacity of this line (approximately 100 times higher than the 22 GHz line) requires a wider range of avoidance around 183 GHz and would only be practical at high sites. Studies of the performance of WVRs at 183 GHz by *Carilli and Holdaway* [1999] and others [*Staguhn et al*., 1998; *Marvel and Woody*, 1998; *Lay*, 1997; *Sutton and Hueckstaedt*, 1996] have been made for use by millimeter interferometers at high sites.

5.3. WVR Pointing Errors

If the WVR is pointed using a mount separate from the VLBI antenna, it must be pointed with high precision or be held fixed for the duration of the VLBI scan. Even with a perfectly uniform atmosphere, jitter in the pointing will result in apparent path length changes due to the variable amount of water vapor in the WVR beam. For example, at an elevation of 20° with a 30 K radiometric temperature from water vapor at the 22.2 GHz line center, a 0.1° elevation error results in a change of 0.14 K, or $\sim$0.6 mm path length. However, the typical pointing error in the VLBI antenna of a few arc seconds results in negligible error.

5.4. Antenna Spillover and Calibration Error

The spillover from the illumination of the WVR and from blockage, in the case of using a dish which is not a clear aperture, can result in a radiometric signature that may be correlated with the water vapor spectrum. In general, however, the spillover is more strongly correlated with a baseline shift or the frequency-squared signature of scattering. Typical total spillover is $\sim$20–30 K and varies slowly with the elevation of the dish. However, more rapid changes can result from the movement of other objects near the WVR and from changes in the atmosphere or ground temperature. For example, if there is a 10% correlation with the water line profile, then we might expect a path length coefficient of $\sim$0.4 mm K^{-1} for changes in ground temperature. The variations produced by the changing location of dish sidelobes as the dish tracks the source might result in 100 mK change or 10 mK of false water vapor signal and 0.04 mm corresponding path length. These "ground pickup" effects have been observed, and in the future we plan to underilluminate the dish by using a larger dish of the same focal length. Accurate calibration is most critical for the absolute measurement of path length. Calibration is far less critical if we are only concerned with measurement of the variations in path length. For example, a 10% error in system temperature calibration changes the retrieval scale by 10%.

5.5. Variations in the "Dry" Refraction

At some level there will be variations in path length produced by refractivity changes in the temperature and pressure of the dry atmosphere. Optical seeing of 1 arc second on a 0.1 m telescope would correspond to a structure function D of baseline length b of

$$D^{1/2}(b) \approx 3 \times 10^{-6} b^{5/6}. \quad (16)$$

Rogers [1988] suggested that 30% of the path variations might be from the dry component as suggested by the coefficient above. However, the outer scale for the dry component is smaller. *Davis et al.* [1995] observed a departure from Kolmogolov turbulence at an outer scale of ~10 m. At this point the rms path length variations approach an asymptotic value of 10 microns, which is less than 3% of the typical wet variations. However, the square root of the structure function may follow an exponent of ⅓, which is appropriate for 2-D turbulence for $b > 10$ m, in which case the rms path variations at a 1 km baseline might reach 50 microns.

5.6. Effect of Liquid Water

A very large wet cloud with 1 g m^{-3} of water droplets 1 km thick is estimated to have a brightness temperature of 20 K at 22 GHz from the liquid water and an excess path of ~4 mm [*Thompson et al.*, 1986, p. 438]. The frequency-squared dependence can be used to estimate this "liquid" path using a scale factor of ~0.2 mm per Kelvin at 22 GHz. The standard deviation of the liquid path from a covariance analysis using the same parameters as in (12) is 0.01 mm. The variations in the liquid path are expected to be less than 10% of the variations due to the water vapor in the same clouds, so it is doubtful that estimation of the liquid path is warranted.

6. Experiments

Data from two separate experiments are shown. The first data set is from Hat Creek interferometer observations of Orion on a baseline of 192 m taken in February 1999 under relatively poor atmospheric conditions. The second data set is from the April 1999, Coordinated Millimeter VLBI Array (CMVA) millimeter VLBI experiment between Hat Creek and Kitt Peak. The weather conditions were moderate at Hat Creek and good at Kitt Peak. The difference when using WVRs to correct the VLBI data is that each site has completely different atmospheres, and the observations are usually at different elevations. In poor weather or very low elevation this can result in a much larger atmospheric effect than seen with a connected element interferometer.

6.1. Connected Element Interferometer

The Hat Creek experiment data are shown in Figure 2. The WVRs were located ~6 m from the center of the 6 m VLBI dishes on their own mounts. This was necessary to avoid blockage and to prevent collisions. However, this offset in the dish centers causes timing errors as the atmosphere flows across both dishes. The WVRs were held stationary for 5 min to avoid the effects of WVR pointing variations. This adds slightly to the offset between beams at times displaced from the center of each 5 min period. These timing errors and beam mismatches are part of the residual phase errors of 0.43 mm. The uncorrected rms phase errors were 0.99 mm. The coherent signal-to-noise ratio (SNR) of this 22 min interferometer scan increases by almost a factor of 3 when the WVR correction is applied. This experiment did demonstrate that our WVRs can work effectively on short baselines, and with future improvements in the pointing, beam matching, fitting, and noise temperature the corrections will improve significantly. A constant scale factor of 4.4 mm K^{-1} was used for the conversion of the WVR data to phase. In all cases we found no significant improvement by adjusting the scale factor.

6.2. Very Long Baseline Interferometer

An example of a scan from the VLBI experiment is shown in Figure 3. In this experiment the WVRs were attached directly to the Kitt Peak and Hat Creek dishes. The WVR at Kitt Peak was attached behind the subreflector, but the WVR at Hat Creek was attached to a dish at the edge of the array, ~50 m from the center of the combined beam. This is equivalent to not correcting the data for a baseline of 50 m. Correcting a phased array spread over 100 m with a single WVR is an added difficulty for VLBI. The phase rms went from 0.88 mm uncorrected to 0.34 mm corrected. These types of direct comparisons of CMVA and WVR phases can only be done on strong sources since high SNR is necessary in the CMVA data to allow removal of phase ambiguities. For both high- and low-SNR scans we applied the WVR corrections to the VLBI phases and compared the coherent fringe amplitude with and without correction. We also computed the maximum attainable fringe amplitude by incoherently averaging VLBI

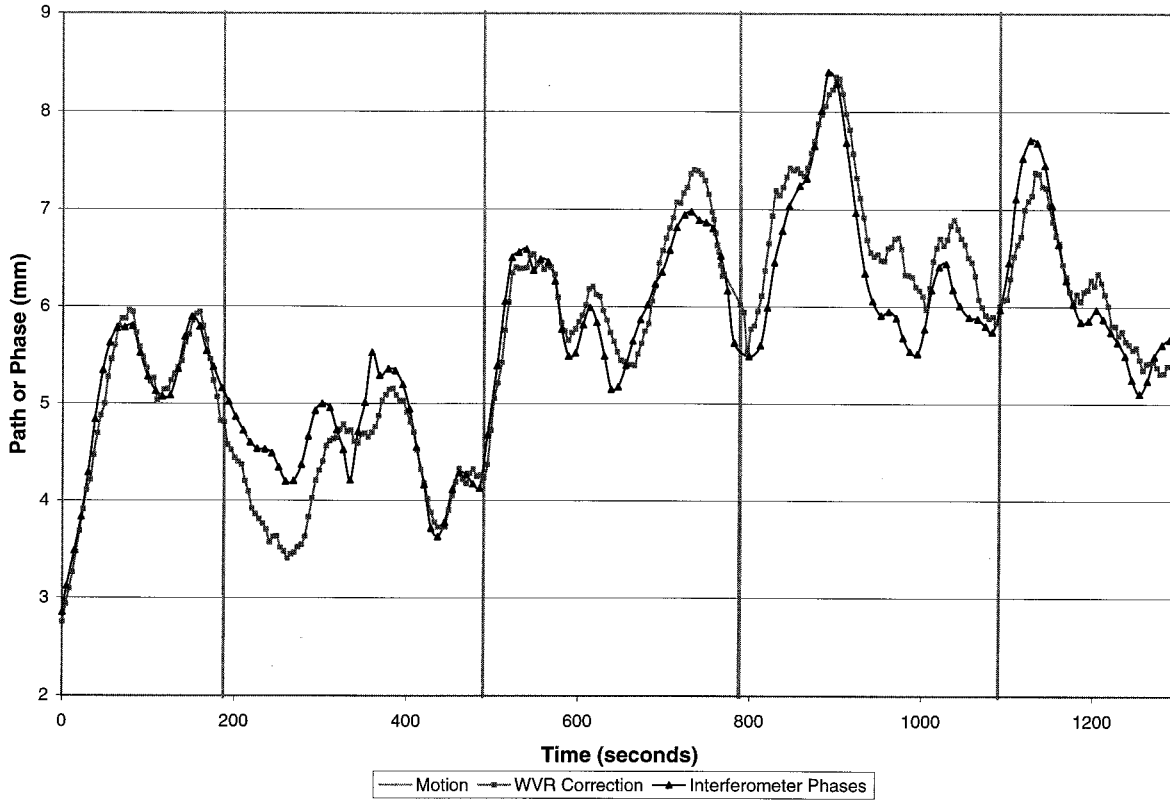

Figure 2. Comparison of Hat Creek interferometer observations of the Orion SiO maser at 86 GHz and WVRs on a baseline of 192 m. The rms phase variations of the interferometer data were reduced from 0.990 to 0.427 mm by incorporating the WVR correction. The interferometer data are the solid triangles, and the WVR data are shaded squares. The vertical lines are at times when the WVRs moved. The coherent SNR increased by a factor of 3 when the WVR correction was applied.

data segments of 10 s coherent integration [*Thompson et al.*, 1986; *Rogers et al.*, 1995]. The ordinate of the data points shown in Figure 4 provides a measure of the improvement in coherence obtained using the WVR-corrected phases. The ordinate is the ratio of the WVR-corrected coherent fringe amplitude to the uncorrected coherent fringe amplitude, the coherent integration being the full 380 s of a VLBI scan. The abscissa is the ratio of the noise-bias-corrected incoherent average of 10 s coherent integrations to the coherent amplitude for each scan. All data points with ordinate above 1 show an improved coherent amplitude with the WVR-corrected phases. The solid line goes through the origin and has unit slope to indicate the maximum possible improvement for which the average amplitude of the noise-bias-corrected segments would equal the coherent amplitude with phase corrections equal to the measured phases. In each case we allowed a new search of the corrected VLBI data for the best fringe rate, but, having no a priori knowledge of time delay, we fixed the time offset at zero. The overall improvement in amplitude was ~20%. The largest improvement is for those cases in which the atmosphere variation is largest, as can be seen by the trend evident in the plot. Figure 4 includes only scans for which fringes were initially detected.

We separately applied WVR corrections to candidate scans for which fringes were not initially detected. We found four candidates that, we estimated, should have an amplitude from just below the detection threshold to ~50% below the threshold on the basis of extrapolation of the observed fringe amplitudes. Of these four scans without initial detections, each having noise peaks around a SNR of 5.0, we detected two with SNRs around 6.5 after applying the WVR corrections. These new detections are consistent with the detection threshold being improved by

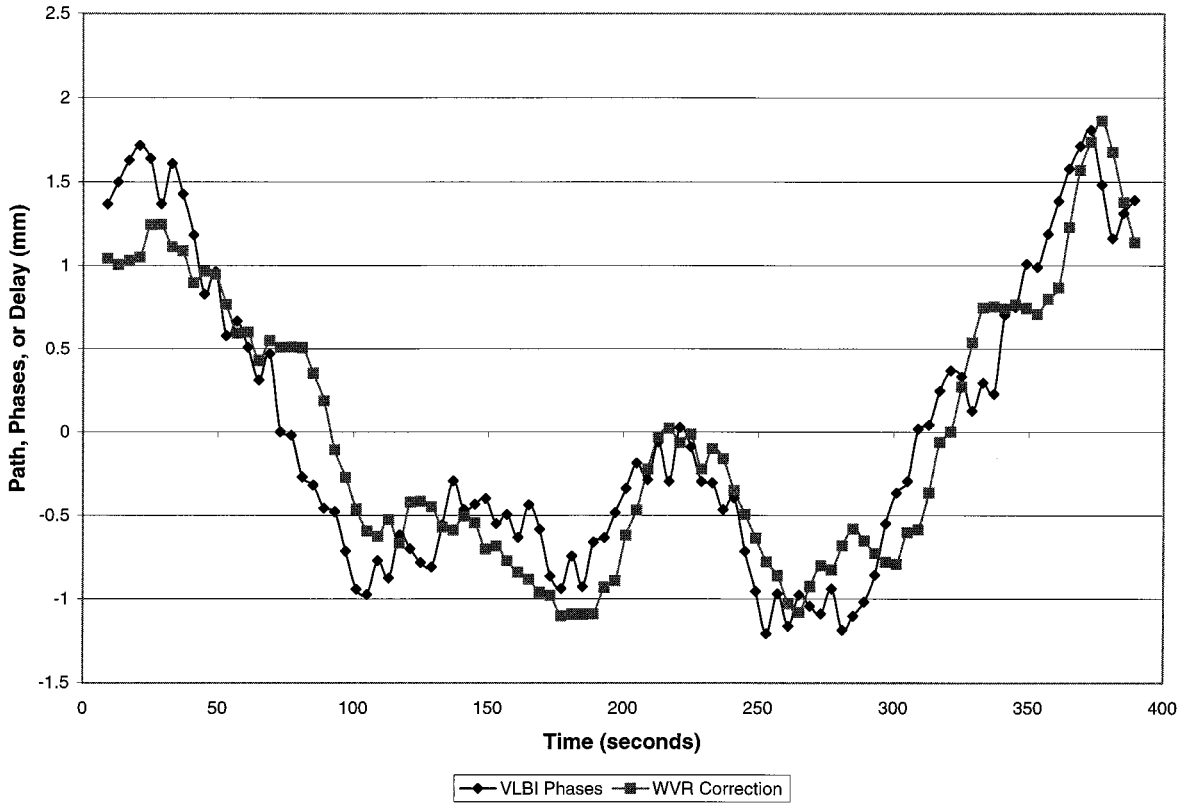

Figure 3. Comparison of CMVA phases on 3C273B and WVR data. The VLBI data are the solid diamonds, and the WVR data are the shaded squares. The rms phase variations of the interferometer data went from 0.88 to 0.34 mm with the WVR correction. The coherent SNR rose by 68%.

~20%. In poorer observing weather we would expect a more dramatic improvement.

6.3. Discussion

If the phase variations σ_0 were distributed with Gaussian statistics, one would expect the correlation to be reduced by the factor

$$e^{-\sigma_0^2/2}, \tag{17}$$

where $\sigma_0 = 2\pi\sigma_d/\lambda$, σ_d is the standard deviation of path length, and λ is the wavelength. In VLBI a "fringe search" is made for the best fringe rate. In this case, for (17) to hold, the standard deviation of path length should be calculated for variations which have been high pass filtered to remove components with frequencies below the inverse of the coherent integration period. Also, for millimeter VLBI there is a significant contribution to the phase variations from the independent hydrogen maser frequency standards at each site. The Allan standard deviation of the masers is 3×10^{-15} at an averaging time of 300 s. If we assume equal performance at each end of the VLBI baseline, we expect (assuming white frequency noise [*Rogers and Moran*, 1981]) an rms path of about

$$\sqrt{2}\ \omega\tau\sigma_A(\tau) \approx 0.4 \text{ mm}$$

where $\omega = 2\pi\nu = 2\pi c/\lambda$, τ is the coherent averaging time, and σ_A is the Allan standard deviation.

If we add quadratically 0.4 mm rms expected for the frequency standards and 0.2 mm rms for the WVR noise, we obtain 0.45 mm rms. Using (17), we would expect the WVR-corrected VLBI data to reach an amplitude of 0.72 times the incoherent amplitude for a coherent integration of 300 s. This expected limit is plotted in Figure 4 as a dash-dotted line with a slope of 0.72. This fits the trend in the data well enough that we feel that the WVR-corrected path variations are consistent with those expected from the combination of frequency standards and noise in the

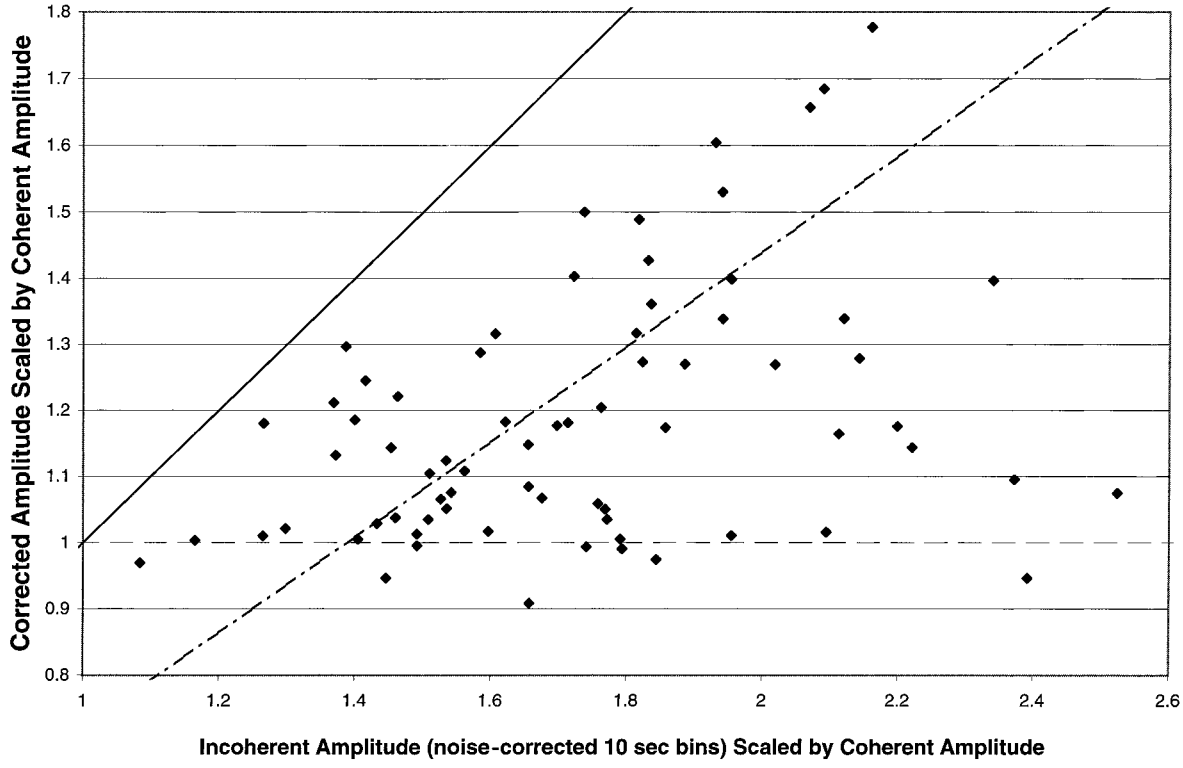

Figure 4. Plot of the ratio of WVR-corrected VLBI amplitude to uncorrected amplitude versus the ratio of incoherent amplitude to uncorrected amplitude. Points with WVR-corrected ratio above 1 were improved by the WVRs. The solid line with unit slope represents the best possible improvement ratio while the dash-dotted line with slope 0.72 represents the average improvement expected while accounting for the phase variations of the frequency standards and noise in WVR measurements. The WVR data were smoothed with 10 s boxcar average, and the incoherent amplitudes were estimated using segments of 10 s duration.

WVRs. Most of the VLBI data were taken during very good weather. The improvements in correlation would be larger for more average weather.

Future improvements in the WVR include using a frequency sequence with less sensitivity to the altitude of the water vapor, lower noise amplifiers, better calibration, and better beam match.

7. Conclusion

The variations in atmospheric path length which severely limit the coherence of millimeter VLBI can be significantly reduced using a very simple and inexpensive WVR spectrometer. This will improve both the quality and reliability of millimeter VLBI observations. Additionally, VLBI observations at 2 mm or 1 mm will be improved, opening up new capabilities in VLBI science. The noise in the WVR, beam offsets, and other systematic error sources currently limit the calibration to timescales longer than 10 s.

Acknowledgments. The authors thank Melvin Wright of the University of California for his interest in the project and his help with testing the WVR performance using the Hat Creek interferometer. We also thank Arthur Niell of Haystack Observatory, Jackie Hewitt of MIT, and the reviewers for their comments. This work was supported by the National Science Foundation (NSF).

References

Armstrong, J. W., and R. A. Sramek, Observations of tropospheric phase scintillations at 5 GHz on vertical paths, *Radio Sci.*, *17*, 1579–1586, 1982.

Carilli, C. L., and M. A. Holdaway, Tropospheric phase calibration in millimeter interferometry, *Radio Sci.*, *34*, 817–840, 1999.

Cruz, S. L., C. S. Ruf, and S. J. Keihm, Improved 20- to 32-GHz atmospheric absorption model, *Radio Sci*., *33*, 1319–1333, 1998.

Davis, J. L., G. Elgered, A. E. Niell, and C. E. Kuehn, Ground-based measurement of gradients in the "wet" radio reflectivity of air, *Radio Sci*., *28*, 1003–1018, 1993.

Davis, J., P. R. Lawson, A. J. Booth, W. J. Tango, and E. D. Thorvaldson, Atmospheric path variations of baselines up to 80 m measured with Sydney University Stellar Interferometer, *Mon. Not. R. Astron. Soc*., *273*, L53–L58, 1995.

Elgered, G., J. L. Davis, T. A. Herring, and I. I. Shapiro, Geodesy by radio interferometry: Water vapor radiometry for estimation of the wet delay, *J. Geophys. Res*., *96*, 6541–6555, 1991.

Hill, R. J., Water vapor–absorption line shape comparison using the 22-GHz line: The Van Vleck–Weisskopf shape affirmed, *Radio Sci*., *21*, 447–451, 1986.

Lay, O. P., Phase calibration and water vapor radiometry for millimeter-wave arrays, *Astron. Astrophys. Suppl. Ser*., *122*, 547–557, 1997.

Linfield, R. P., and J. Z. Wilcox, Radio metric errors due to mismatch and offset between a DSN antenna beam and the beam of a troposphere calibration instrument, *NASA/JPL Telecommun. Data Acquisition Prog. Rep*., *42-114*, 1993.

Linfield, R. P., S. J. Keihm, L. P. Teitelbaum, S. J. Walter, M. J. Mahoney, R. N. Truehaft, and L. J. Skjerve, A test of water vapor radiometer based troposphere calibration using very long baseline interferometry on a 21-km baseline, *Radio Sci*., *31*, 129–146, 1996.

Marvel, K., and D. Woody, Phase correction at millimeter wavelengths using observations of water vapor at 22 GHz, in *Advanced Technology MMW, Radio, and Terahertz Telescopes*, edited by T. Phillips, *Proc. SPIE Int. Soc. Opt. Eng*., *3357*, 442–452, 1998.

Rogers, A. E. E., Atmospheric Limits: A review of the effect of the path length variations on the coherence and accuracy of VLBI, *Symp. Int. Astron. Union*, *129*, 533–540, 1988.

Rogers, A. E. E., and J. M. Moran, Coherence limits for very-long-baseline interferometry, *IEEE Trans. Instrum. Meas*., *IM-30*, 283–286, 1981.

Rogers, A. E. E., A. J. Moffet, D. C. Backer, and J. M. Moran, Coherence limits in VLBI observations at 3-millimeter wavelength, *Radio Sci*., *19*, 1552–1560, 1984.

Rogers, A. E. E., S. S. Doeleman, and J. M. Moran, Fringe detection methods for very long baseline arrays, *Astron. J*., *109*, 1391–1401, 1995.

Rosenkranz, P. W., Water vapor microwave continuum absorption: A comparison of methods and models, *Radio Sci*., *33*, 919–928, 1998.

Staguhn, J., A. Harris, R. L. Plambeck, and W. J. Welch, Phase correction for the BIMA array: Atmospherical model calculations for the design of a prototype correlation radiometer, in *Advanced Technology MMW, Radio, and Terahertz Telescopes*, edited by T. Phillips, *Proc. SPIE Int. Soc. Opt. Eng*., *3357*, 432–441, 1998.

Sutton, E. C., and R. M. Hueckstaedt, Radiometric monitoring of atmospheric water vapor as it pertains to phase correction in millimeter interferometry, *Astron. Astrophys. Suppl. Ser*., *119*, 559–567, 1996.

Thayer, G. D., An improved equation for the radio refractive index of air, *Radio Sci*., *9*, 803–807, 1974.

Thompson, A. R., J. M. Moran, and G. W. Swenson, *Interferometry and Synthesis in Radio Astronomy*, John Wiley, New York, 1986.

Truehaft, R. N., and G. E. Lanyi, The effect of the dynamic wet troposphere on radio interferometric measurements, *Radio Sci*., *22*, 251–265, 1987.

Waters, J. W., Absorption and emission by atmospheric gases, in *Methods of Experimental Physics*, vol. 12B, *Astrophysics*, edited by M. L. Meeks, pp. 142–176, Academic, San Diego, Calif., 1976.

A. Rogers and D. A. Tahmoush, Haystack Observatory, Massachusetts Institute of Technology, Route 40, Westford, MA 01886. (aeer@newton.haystack.edu; dtahmoush@haystack.mit.edu)

(Received February 11, 2000; revised July 12, 2000; accepted July 14, 2000.)